AIP | APL Materials

Research Update: Strategies for efficient photoelectrochemical water splitting using metal oxide photoanodes

Seungho Cho, Ji-Wook Jang, Kun-Hong Lee, and Jae Sung Lee

Citation: APL Materials **2**, 010703 (2014); doi: 10.1063/1.4861798
View online: http://dx.doi.org/10.1063/1.4861798
View Table of Contents: http://scitation.aip.org/content/aip/journal/aplmater/2/1?ver=pdfcov
Published by the AIP Publishing

APL MATERIALS **2**, 010703 (2014)

Research Update: Strategies for efficient photoelectrochemical water splitting using metal oxide photoanodes

Seungho Cho,[1] Ji-Wook Jang,[2] Kun-Hong Lee,[2,a] and Jae Sung Lee[3,a]
[1]*Department of Chemistry and Pohang University of Science and Technology (POSTECH), San 31, Hyoja-Dong, Nam-Gu, Pohang, Gyungbuk 790–784, South Korea*
[2]*Department of Chemical Engineering, Pohang University of Science and Technology (POSTECH), San 31, Hyoja-Dong, Nam-Gu, Pohang, Gyungbuk 790–784, South Korea*
[3]*School of Energy and Chemical Engineering, Ulsan National Institute of Science and Technology (UNIST), 50 UNIST-gil, Ulsan 689–798, South Korea*

(Received 4 November 2013; accepted 30 December 2013; published online 31 January 2014)

Photoelectrochemical (PEC) water splitting to hydrogen is an attractive method for capturing and storing the solar energy in the form of chemical energy. Metal oxides are promising photoanode materials due to their low-cost synthetic routes and higher stability than other semiconductors. In this paper, we provide an overview of recent efforts to improve PEC efficiencies via applying a variety of fabrication strategies to metal oxide photoanodes including (i) size and morphology-control, (ii) metal oxide heterostructuring, (iii) dopant incorporation, (iv) attachments of quantum dots as sensitizer, (v) attachments of plasmonic metal nanoparticles, and (vi) co-catalyst coupling. Each strategy highlights the underlying principles and mechanisms for the performance enhancements. [http://dx.doi.org/10.1063/1.4861798]

Solar water splitting for production of dihydrogen as an energy carrier by using only water and sun light, omnipresent and sustainable resources on the Earth is extremely attractive. Nature already uses this attractive approach using chlorophyll-containing proteins with two coupled photosystems, photosystem II and photosystem I, to absorb sun light and split water into oxygen and NADPH.[1] Hydrogen is a promising energy carrier due to its high energy content per unit mass (120 J/g, ca. 3 times that of gasoline) and clean combustion product (only water) in a CO_2-neutal manner.[2] Currently, the main commercial process for hydrogen production is steam reforming of hydrocarbons, resulting in problematic CO_2 emission.[3]

Solar water splitting can be achieved by three representative methods: electrolysis powered by photovoltaics, particulate photocatalysis, and photoelectrochemical (PEC) water splitting. Photovotaic-electrolysis is a high-efficiency, yet high-cost method. Currently, the main challenge faced by the community is the dilemma between efficiency and cost.[4] Nature using an extremely large scale of natural photosynthesis suggests that a cost-effective route is indispensable for commercialization of solar water splitting. Particulate photocatalysis is a low-cost system. However, separation of the explosive hydrogen and oxygen gas mixture is needed, which will consume energy additionally reducing the overall water splitting efficiency. Metal co-catalysts used for hydrogen and oxygen production from water are often good catalysts for the recombination of hydrogen and oxygen as well, which can reduce net water splitting efficiency.[5] In addition, both conduction and valence band positions should be well matched with the hydrogen and oxygen evolution potential to split water (i.e., overall water splitting).

[a]Authors to whom correspondence should be addressed. Electronic addresses: jlee1234@unist.ac.kr and ce20047@postech.ac.kr

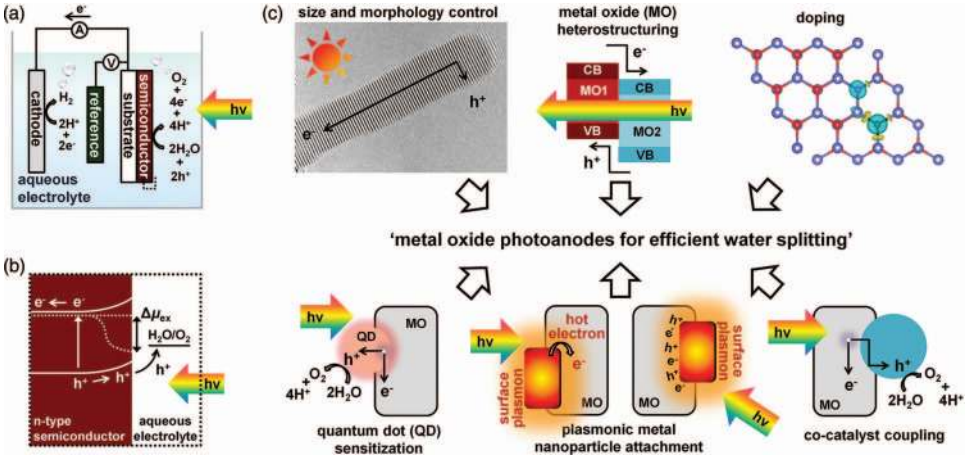

FIG. 1. (a) Schematic diagram of a photoelectrochemical water splitting cell. (b) Electron energy scheme of a n-type semiconductor in an aqueous electrolyte. (c) Strategies for efficient metal oxide photoanodes.

Photoelectrochemical water splitting, demonstrated first by Fujishima and Honda,[6] possesses a potential high efficiency (up to >30% in principle) and is a relatively low-cost method.[2,7] Gaseous H_2 and O_2 are generated at the cathode and anode, respectively as illustrated in Figure 1(a). Because half reactions of H_2 or O_2 evolution can be physically separated, PEC water splitting does not require additional hydrogen and oxygen separation process and allows each to be optimized independently. Although the reduction reaction producing H_2 must occur to complete PEC water splitting, the efficient operation of the water oxidation reaction (oxygen evolution and H^+ formation) is a fundamental requirement to obtain PEC solar fuels at high solar-to-hydrogen (STH) efficiency.[8] Metal oxides are promising materials for the PEC applications especially for the photoanode performing the oxidation half reaction, due to their higher stability than other semiconductors. In addition, well-established low-cost routes can prepare a variety of oxide semiconductors with a wide range of optoelectronic properties that are closely related to the diversity of cation oxidation states, crystal structures, and electronic configurations associated with the oxides.[9]

Many reviews have been published based on significant progress in PEC water splitting over the past several decades.[2,4,8–18] In this paper, we will focus on recent research efforts for efficient metal oxide PEC photoanodes through various strategies with emphasis on our own studies. Advances on metal oxide-based photoanodes composed of all inorganic materials are reviewed, excluding organic materials as decorations of metal oxides for enhanced efficiencies, such as dye-sensitization, molecular catalyst, or enzyme. Starting with a brief introduction to PEC water splitting reactions, we overview the strategies for efficient PEC water oxidation using metal oxide photoanodes.

Water splitting into H_2 and O_2 is an uphill reaction, requiring an energy input, with a Gibbs free energy of 237 kJ mol^{-1}.[1] A typical PEC water splitting device employs a photoanode and cathode immersed in an aqueous electrolyte although a photocathode and light-inactive anode can be also used. The cleavage of water molecules to form O_2 and H_2 involves the redox half reactions shown in Eqs. (1) and (2):[11]

$$2H_2O(l) \rightarrow O_2(g) + 4H^+(aq) + 4e^-,\ E_{red}{}^\circ = 1.23V\ (\text{vs. RHE}), \quad (1)$$

$$4H^+(aq) + 4e^- \rightarrow 2H_2(g),\ E_{red}{}^\circ = 0V\ (\text{vs. RHE}). \quad (2)$$

Typically, *n*-type semiconductors are used as photoanodes in contact with aqueous redox electrolytes as illustrated in Figure 1(b). Electrons are transferred from a semiconductor into an aqueous redox electrolyte until the Fermi energy levels equalize, which creates a space charge region across the interface, giving rise to bending of the conduction and valence bands of the semiconductor (upward for *n*-type semiconductor, Figure 1(b)). A balancing charged layer is formed in the electrolyte. This charged layer is usually taken up within the first few monolayers of solvent molecules in a region

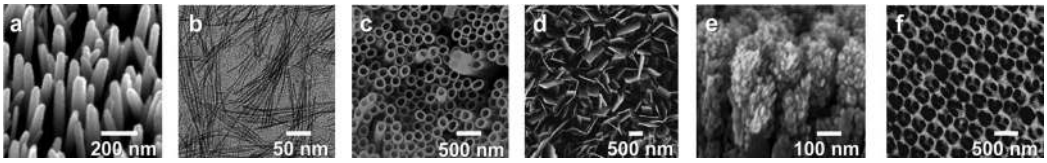

FIG. 2. Electron microscope images of photoanodes based on nanomaterials with various morphologies: (a) ZnO rods, (b) WO_3 wires,[28] (c) TiO_2 tubes,[34] (d) WO_3 plates,[37] (e) α-Fe_2O_3 dendritic structures,[39] and (f) Bi_2WO_6 inverse opal.[40] Reproduced by permission from R. H. Goncalves, L. D. T. Leite, and E. R. Leite, ChemSusChem **5**, 2341 (2012). Copyright 2012 Wiley-VCH. Reproduced by permission from M. Paulose, K. Shankar, S. Yoriya, H. E. Prakasam, O. K. Varghese, G. K. Mor, T. A. Latempa, A. Fitzgerald, and C. A. Grimes, J. Phys. Chem. B **110**, 16179 (2006). Copyright 2006 American Chemical Society. Reproduced by permission from F. Amano, M. Tian, G. Wu, B. Ohtani, and A. Chen, ACS Appl. Mater. Interfaces **3**, 4047 (2011). Copyright 2011 American Chemical Society. Reproduced by permission from A. Kay, I. Cesar, and M. Gratzel, J. Am. Chem. Soc. **128**, 15714 (2006). Copyright 2006 American Chemical Society. Reproduced by permission from L. W. Zhang, C. Baumanis, L. Robben, T. Kandiel, and D. Bahnemann, Small **7**, 2714 (2011). Copyright 2011 Wiley-VCH.

called the Helmholtz layer which sustains a large electric field due to the small permittivities of electrolytes.[19] Upon illumination, the Fermi level is split into the hole and electron quasi-Fermi levels, which generates an electrochemical potential $\Delta\mu_{ex}$ between the semiconductor-electrolyte junction and the cathode (Figure 1(b)). To achieve PEC water splitting, $\Delta\mu_{ex}$ per electron should be greater than the 1.23 V, the thermodynamic potential required to split water plus some overpotentials. The practical limit of $\Delta\mu_{ex}$ is thought to be ca. 2.0 eV,[12] which leaves out much of the solar spectrum and reduces the maximum practically achievable efficiency to less than 10% under sunlight if using a single light absorber.[5]

Four fundamental steps determine the overall performance for PEC water splitting:[2] (i) light absorption and charge carrier generation, (ii) charge separation, (iii) charge transport, and (iv) charge carrier extraction and electrochemical product formation. Thus, STH efficiency (η_{STH}) can be expressed as Eq. (3):

$$\eta_{STH} = \eta_A \times \eta_{CS} \times \eta_{CT} \times \eta_{CR}, \tag{3}$$

where η's represent efficiencies of light absorption (η_A), charge separation (η_{CS}), charge transport (η_{CT}), and charge collection/reaction efficiency (η_{CR}). To achieve a high STH efficiency of a PEC system, the efficiency of each step should be improved. The carefully scrutinized design of efficient photoanodes is crucial to improve the efficiencies. Fruitful strategies applied to metal oxide photoanodes have been developed to improve the efficiency of each step and consequently the overall STH efficiency including (i) size- and morphology-controlling, (ii) metal oxide heterostructuring, (iii) doping, (iv) quantum dot sensitization, (v) plasmonic metal nanoparticle attachment, and (vi) co-catalyst coupling as schematically summarized in Figure 1(c).

Electronic or optical properties of materials in particular semiconductors can be strongly dependent on their sizes or morphologies. Efforts for size- and morphology-control of metal oxides as photoanodes have been made primarily to reduce photogenerated carrier recombination. In general, materials with nanometer length scales have emerged as efficient components of PEC cells because charge carriers are generated near the surface, where water splitting reactions take place, due to their high surface-to-volume ratios. The nanoscale effects could give rise to 50%–90% efficiency gain.[5] In addition to the size reduction effects, shapes of metal oxide photoanode materials have been tailored (Figure 2) (i.e., "morphology control" of "nanostructures") because their morphologies can also substantially influence PEC efficiency.

One-dimensional (1D) nanostructures including nanorods, nanowires, and nanotubes are very attractive for PEC photoanodes (Figures 2(a)–2(c)). They can decouple the directions of charge collection and light absorption. Their small radial dimensions can minimize the distance for holes to diffuse to the photoanode surfaces. Their relatively large axial dimentions should allow increase in optical path lengths and vectorial, or directional, electron transport along the long axis.[2,20] These merits stimulate efforts to develop photoanodes based on 1D metal oxide nanostructures. Early works for PEC water splitting using 1D metal oxides employed α-Fe_2O_3 nanorod arrays as

photoanodes.[21,22] These approaches were extended to other metal oxide photoanodes for efficient charge transport such as TiO_2 nanorods,[23] TiO_2 nanowires,[24] ZnO nanorods,[25] ZnO nanowires,[26] WO_3 nanorods,[27] WO_3 nanowires,[28] and $PbBi_2Nb_2O_9$ nanorods.[29] Nanorod or nanowire arrays allowed a more efficient transport and collection of photogenerated electrons through a designed path compared to planar films.[21,24–26]

Nanotubes have less material for light absorption but higher surface area for redox reactions in comparison with nanorods or nanowires.[2,30] α-Fe_2O_3 nanotube array photoanodes were prepared via electrochemical anodization of iron foils and subsequent annealing for crystallization.[31,32] Thus, LaTempa *et al.* reported α-Fe_2O_3 nanotubes prepared by anodization of an iron foil in an ethylene glycol electrolyte containing NH_4F and deionized water and their PEC properties.[31] Mohapatra *et al.* prepared photoanodes composed of thin α-Fe_2O_3 nanotubes by a sonoelectrochemical anodization method.[32] A photocurrent density of ca. 1 mA cm^{-2} at 1.23 V (vs. RHE) was achieved for the photoanodes under AM1.5 illumination (87 mW cm^{-2}). TiO_2 nanotube photoanodes were also fabricated by anodization and subsequent annealing.[33,34] The wall thickness and length of the nanotubes could be controlled by varying anodization conditions. The nanotube wall thickness was found to be an important parameter that influences the magnitude of the photoanodic response and the overall efficiency of the water splitting reaction.[33] Mor *et al.* demonstrated H_2 generation at an overall conversion efficiency of 6.8% under 320–400 nm UV illumination (100 mW cm^{-2}).[33] Paulose *et al.* fabricated TiO_2 nanotube arrays having lengths up to 134 μm.[34] In initial measurements, 45 μm long nanotubes arrays exhibited a high water photoelectrolysis photoconversion efficiency of 16.25% at −0.52 V (vs. Ag/AgCl) under 320–400 nm UV illumination (100 mW cm^{-2}).

Two-dimensional (2D) metal oxide nanostructures have been used as photoanode materials for water oxidation.[35–38] The 2D nanostructures have high surface areas and their small thicknesses reduce the distance for photogenerated holes to diffuse to the surfaces, which allows an efficient light harvesting. Platelet-like α-Fe_2O_3 (with thicknesses of 5–10 nm) photoanodes were fabricated by ultrasonic spay pyrolysis which exhibited enhanced photoresponse compared to those deposited by the conventional spray pyrolysis method (planar films).[35] The 2D WO_3 photoanodes were prepared by hydrothermal methods (Figure 2(d)).[37,38] Amano *et al.* observed the thickness of the film strongly influenced the process of photoexcited electron transport.[37] Three-dimensional (3D) nanostructures are also promising building blocks for designing high-performance photoanodes. Dendritic α-Fe_2O_3 nanostructure photoanodes were fabricated by an atmospheric pressure chemical vapor deposition (APCVD) method (Figure 2(e)).[39] Water was oxidized on the photoanode with an incident-photon-to-current-efficiency (IPCE) of 42% at 370 nm and 2.2 mA/cm^2 at 1.23 V (vs. RHE) under AM1.5 100 mW cm^{-2} simulated sunlight. The authors attributed the high efficiency in part to the dendritic nanostructure which minimized the distance photogenerated holes have to diffuse to reach the α-Fe_2O_3/electrolyte interface while still allowing efficient light absorption.

Photonic crystals have attracted extensive interest for their potential applications in manipulating light in nontraditional ways based on photonic band-structure concepts.[40–44] Slow photons propagating with strongly reduced group velocity found in photonic crystals have an immense potential for increasing the path length of light.[45] Therefore, the photonic crystals can promote light absorption, resulting in photogenerated charge carriers. The 3D inverse opal photonic crystals with large surface areas have been constructed for the improvement of electron transport and light harvesting.[46–49] Inverse opal structured α-Fe_2O_3 and Bi_2WO_6 were constructed as photoanodes of PEC cells for efficient solar water splitting (Figure 2(f)).[40,46] The inverse opal-based photoanodes showed more than 2-fold enhanced photon-to-hydrogen conversion efficiencies of PEC water splitting as compared with the corresponding conventional films. The size and morphology control discussed in this section forms the basis for other strategies presented below.

All-metal oxide heterostructured photoanode systems have been widely developed due to relatively high stabilities of metal oxides immersed in aqueous electrolytes and their following characteristics: (i) Basically, heterostructuring of metal oxides with distinctive band gaps can extend the spectral range of light absorption; (ii) Type-II band offsets[50] of two metal oxide components can promote the efficient separation of photogenerated electrons and holes under light irradiation; and (iii) Metal oxide heterostructuring can be also utilized as effective

tools towards passivating surface states, maintaining nanostructures and preventing dissolution in electrolytes.

Heterostrucrures composed of various combinations of metal oxides have been reported to facilitate charge carrier separations at their heterojunctions for efficient PEC water oxidation, such as TiO_2/α-Fe_2O_3,[51] α-$Fe_2O_3/SrTiO_3$,[52] $Fe_2O_3/ZnFe_2O_4$,[53] $TiO_2/ZnFe_2O_4$,[54] TiO_2/WO_3,[55–57] $WO_3/BiVO_4$,[58,59] and $TaON/CaFe_2O_4$.[60] The metal oxide combinations have proper positions of conduction and valence band edges to form potential gradients at the interfaces leading to enhancing the charge separation and inhibiting the recombination rate. Consequently, their overall PEC efficiencies increase compared to the individual single component case.

Surface recombination at trapping states has been thought to be an important factor contributing to the overpotential.[61] α-Fe_2O_3 were passivated with metal oxides of the corundum structure, such as Al_2O_3, Ga_2O_3, and In_2O_3,[61,62] exhibiting cathodic onset potential shifts of 0.1–0.2 V and enhanced photocurrent densities in comparison with those of α-Fe_2O_3 before heterostructuring. It was proposed that the corundum overlayers released lattice strain of the α-Fe_2O_3 layer and decreased the density of surface states.[62] Electrochemical impedance and photoluminescence spectroscopy revealed a significant change in the surface capacitance and radiative recombination, respectively, which distinguishes the observed overpotential reduction from a catalytic effect and confirms the passivation of surface states.[61]

A relatively high electron mobility of ZnO (205–300 $cm^2\ V\ s^{-1}$ vs. 0.1–4 $cm^2\ V\ s^{-1}$ for TiO_2) reduces the electrical resistance and enhances the electron transfer efficiency[63,64] indicating that ZnO should be useful as a highly efficient PEC photoanode component. However, the chemical stability of ZnO in an aqueous electrolyte is relatively poor because of its amphoteric characteristic. To address this limitation, surface coating of ZnO nanowires by anti-corrosive shell layers with photocatalytic activities has been investigated.[65] Hence, $ZnO/ZnGa_2O_4$ core/shell heterostructured nanowire photoanodes were fabricated by a two-step CVD method. A *stable* photocurrent of 1.2 mA cm^{-2} was obtained with the heterostructure array as a photoanode at 0.7 V (vs. Ag/AgCl) under a 300 W xenon lamp illumination, which suggests that the $ZnGa_2O_4$ shells provided an anti-photocorrosion ability. Jun *et al.* used α-Fe_2O_3/Al_2O_3 heterostructures for preparation of honeycomb-like α-Fe_2O_3 films to prevent agglomeration of the α-Fe_2O_3 during the annealing process for improving their crystallinity, which is essential for high photocatalytic performance of α-Fe_2O_3 although Al_2O_3 layers were removed prior to PEC water splitting.[66] Through heterostructuring, α-Fe_2O_3 nanostructure was preserved after annealing at 550 °C. This highly ordered nanostructure film exhibited much enhanced PEC cell performances relative to α-Fe_2O_3 films with low degrees of ordering.

Doping is an effective way to Taylor electronic and optical properties of metal oxide semiconductors. Incorporation of cations or anions into metal oxide matrices have been investigated to enhance PEC water splitting efficiencies through a variety of dopant effects such as electrical conductivity enhancements, intra-band gap state formations and band gap narrowing.

α-Fe_2O_3 photoanodes doped with cations, such as Si, Ti, Pt, Cr, Mo, and Al, showed enhancements in photocurrent densities.[67–69] The reports suggested various mechanisms underlying the enhanced PEC efficiency of the α-Fe_2O_3 photoanodes by cation doping. Glasscock *et al.* reported Si- or Ti-doped α-Fe_2O_3 films prepared using magnetron sputtering and their significantly higher PEC activities than the undoped material.[67] Based on the results of film characterizations, the authors attributed the enhanced photocurrent densities to reduction of recombination due to an improvement in the charge transfer rate at the surface and passivation of the grain boundaries by the dopants. Hu *et al.* demonstrated that Pt doping can increase photocurrent density.[68] The linear dependence of photocurrent density on light intensity was cited as evidence of recombination rate reduction in comparison with the undoped case. Electrochemical methods for preparing Cr- or Mo-doped α-Fe_2O_3 have been reported.[69] The IPCE values were ca. 2-fold and 4-fold higher than the undoped sample for the 5% Cr and 15% Mo samples, respectively, which were attributed to an improvement in the charge transport properties.

Recently, visible light-induced water oxidation activities of 12 metal ion-doped $BiVO_4$ were investigated (Figure 3(a)).[70] In the case of W and Mo doping, the activities were dramatically enhanced. The highest photocurrent densities of 2.38 mA cm^{-2} and 1.98 mA cm^{-2} were achieved for Mo and W doping at 1.23 V (vs. RHE) under simulated AM1.5 illumination, respectively,

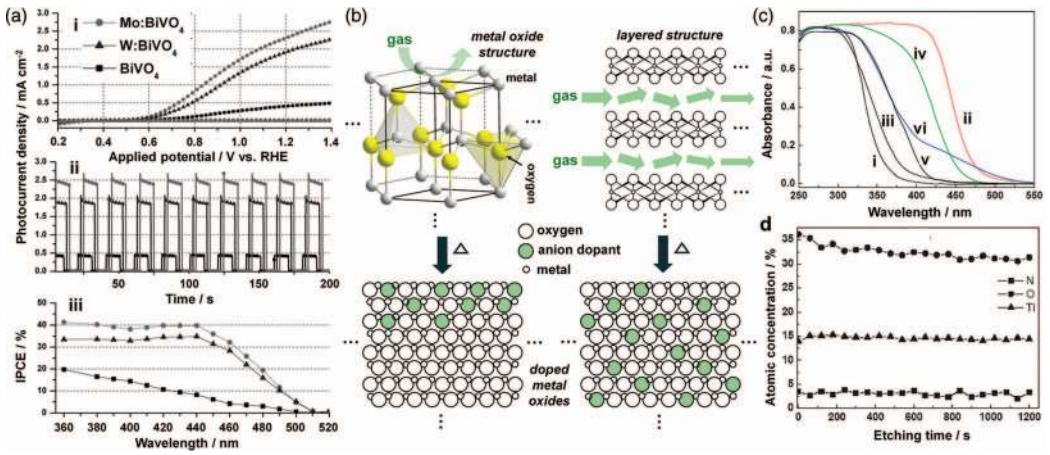

FIG. 3. (a): (i) Photocurrent-potential curves, (ii) time-dependent photocurrent densities at 1.23 V (vs. RHE) were recorded under 1 sun (100 mW cm^{-2}) 0.1 M aqueous solution of Na_2SO_4, and (iii) incident photon-to-current conversion efficiency spectra of the photoanodes.[70] Reproduced by permission from K. P. S. Parmar, H. J. Kang, A. Bist, P. Dua, J. S. Jang, and J. S. Lee, ChemSusChem **5**, 1926 (2012). Copyright 2012 Wiley-VCH. (b) Schematic diagram showing easy access of a post treatment gas to the precursors in the cases of layered structure relative to bulk structure. (c) UV-visible light absorption spectra of (i) $Cs_{0.68}Ti_{1.83}O_4$, (ii) $Cs_{0.68}Ti_{1.83}O_{4-x}N_x$, (iii) $H_{0.68}Ti_{1.83}O_4$, (iv) $H_{0.68}Ti_{1.83}O_{4-x}N_x$, (v) commercial P25, and (vi) N-doped P25.[82] (d) XPS depth profiles of the elements of Ti, O, and N in the $H_{0.68}Ti_{1.83}O_{4-x}N_x$ upon Ar^+ sputtering.[82] Reproduced by permission from G. Liu, L. Z. Wang, C. H. Sun, X. X. Yan, X. W. Wang, Z. G. Chen, S. C. Smith, H. M. Cheng, and G. Q. Lu, Chem. Mater. **21**, 1266 (2009). Copyright 2009 American Chemical Society.

whereas undoped $BiVO_4$ yielded a photocurrent value of 0.42 mA cm^{-2}. Mott–Schottky analysis and electrochemical impedance spectroscopy indicated a positive flat band shift of ca. 30 mV, 1.6–2-fold higher carrier concentrations and 3–4-fold reduced charge-transfer resistances for the Mo- or W-doped $BiVO_4$ compared to the undoped case.

Anion doping has been investigated for realizing visible light photocatalytic activities of wide band gap metal oxides by formations of intra-band gap states or band gap narrowing. In the case of TiO_2 and ZnO, their valence band edges are far below the water oxidation energy level. By C or N doping, for example, the valence band edges can be elevated by formations of hybridized orbitals of O 2p states and C or N 2p states,[71] and/or the localized states of C 2p or N 2p may be generated within the band gap,[72] because the C 2p and N 2p states have higher orbital energies than the O 2p state, while keeping the conduction band edges almost unaltered.[73]

TiO_2 photoanodes has been doped by anions such as C and N for visible light activities. Kahn *et al.* fabricated C-doped TiO_2 photoanodes by pyrolysis of Ti metal sheets in natural gas flames at ca. 850 °C.[74] This photoanode absorbed light at wavelengths below 535 nm and has a much smaller band-gap energy (2.32 eV) than rutile TiO_2 (3.03 eV).[75] The visible light-active electrode showed enhanced PEC efficiency compared with undoped TiO_2 structures. C-doping of TiO_2 by carbonaceous gas treatments of already synthesized TiO_2 nanotubes have been reported. Park *et al.*[76] and Raja *et al.*[77] incorporated C into TiO_2 nanotubes by annealing in a CO atmosphere up to 700 °C and in an C_2H_2-H_2 gas mixture at 650 °C, respectively. The C-doped photoanodes showed red-shifted absorption spectra and enhanced water splitting efficiencies under visible light irradiations in comparison with the corresponding pure TiO_2 nanotubes. N-doped TiO_2 was prepared by annealing the TiN thin film in air.[78] PEC measurements demonstrated visible light photoresponse for the N-doped TiO_2. Recently, N-doped TiO_2 nanowire array photoanodes prepared by nitridation of pure TiO_2 nanowire arrays in NH_3 flow at 500 °C (i.e., post-treatments) were reported.[79] The low-energy threshold of the IPCE spectra of the N-doped TiO_2 samples was at ca. 520 nm corresponding to 2.4 eV.

Yang *et al.* reported N-doped ZnO nanowire arrays synthesized by a hydrothermal method for the ZnO synthesis followed by annealing in NH_3 flow for N doping.[80] The PEC measurements showed visible light photoresponse and an-order-of-magnitude increase in photocurrent density with STH conversion efficiency of 0.15% at an applied potential of 0.5 V (vs. Ag/AgCl) under AM1.5

irradiation in comparison with the pristine undoped ZnO nanowire arrays. By a similar post thermal nitridation process, a photoanode based on N-doped ZnO nanotetrapods was investigated, which features visible light activity, vectorial electron transport, network formation ability, and increased roughness factor for boosting light harvesting.[81]

As discussed above, anion doping has been realized by post-treatments of already fabricated metal oxide photoanodes. However, in general, dopants incorporated by the post-treatments are distributed mainly within the subsurface region of a very limited depth (Figure 3(b)).[73,82] Limitations are caused by this non-uniform dopant distribution, such as limited visible-light absorbance[79,80] and lowered mobility of carriers in the localized states, which deteriorate visible-light photocatalytic activities.[71,82] To overcome the limitations, Liu *et al.* used layered materials with interlayer galleries, layered titanates, as host materials for N doping by nitridation, giving products that possess a band-to-band visible light absorption edge in the blue light region via the homogeneous substitution of O by N although the products were not applied to photoanode materials (Figures 3(c) and 3(d)).[82] Cho *et al.* reported ZnO and $ZnAl_2O_4$ mixed metal oxide (MMO) nanostructures co-doped uniformly by C and N synthesized by thermal nitridation of a terephthalate-intercalated layered double hydroxides with interlayer galleries.[73] The anion-doped MMOs exhibited significantly red-shifted absorption spectra to visible light region relative to pure MMOs and ZnO nanoplates doped by the identical nitridation process. PEC water oxidation and IPCE data demonstrated that all the visible light absorption brought by the anion doping contributed to the photocatalytic activity over the entire absorbed wavelength range of <610 nm.

As mentioned, anion doping is usually intended for band gap narrowing of wide band gap metal oxides by modification of their valence band positions. But it can also bring improvement in the charge transport properties such as doping of metal cations. In a lone example, Jo *et al.* doped a monoclinic $BiVO_4$ lattice with phosphate to enhance PEC water oxidation activity under visible light by a factor of about 30 compared with pristine $BiVO_4$.[83] Electrochemical impedance spectroscopy measurements and density functional theory calculations revealed that much improved charge transfer characteristics of $BiVO_4$ were mainly responsible for the greatly enhanced photoelectrochemical activity.

Quantum dots (QDs), semiconducting nanocrystals, are promising "sensitizers" because of the following reasons:[84–86] (i) flexible tunability of the band gap across UV, visible and infrared (IR) region, (ii) broad absorption with high molar absorptivity, (iii) robustness against photobleaching, and (iv) salient phenomena such as multiple excition generation[87] and energy-transfer-assisted charge collection.[88] Based on such promising characteristics, QDs have been used as sensitizers for PEC water splitting applications in particular photoanode parts (e.g., wide band gap *n*-type metal oxides). Efficient electron injection from a visible light-active QD to a metal oxide requires that the conduction band edge of the QD is located above that of the metal oxide.[89] The electron transfer between the QD and the metal oxide can facilitate the charge separation and inhibit recombination through a potential gradient at the interface.[2]

Attachments of QDs on metal oxide surfaces can be achieved by (i) *in situ* growth and (ii) post-synthesis assembly. *In situ* growth generally facilitates charge carrier transfer across the interfaces between QDs and metal oxides due to their direct contact in atomic scale. On the other hand, the post-synthesis assembly enables maximal control over the size, size distribution, and surface functionalization of QDs.[90] Thus, their band gap, the density and energy of their trap states, the driving forces of interfacial charge-transfer processes, and the distance and electronic coupling between QDs and metal oxides can be finely tailored.

In situ cadmium chalcogenide QD formations by electrodeposition, chemical bath deposition or successive ionic layer adsorption, and reaction routes on various nanostructure arrays (e.g., nanotubes, nanowires, nanorods, and inverse opal) of TiO_2,[91,92] ZnO,[93,94] or TiO_2/ZnO (core/shell)[95] for PEC photoanodes have been reported. Visible light absorption of the QDs and type-II band edge configuration promoting spatial separation of photogenerated carriers could significantly enhance PEC water oxidation efficiencies under simulated sunlight. Zinc chalcogenide QDs, less toxic than cadmium chalcogenide QDs, were also used as sensitizers. Cho *et al.* synthesized ZnSe-decorated ZnO nanowire photoanodes by a dissolution-recrystallization process.[96] The ZnO/ZnSe photoanodes exhibited absorption in the visible spectrum (<550 nm in wavelength) and photocurrent

enhancements under simulated AM1.5 solar light compared to the pristine ZnO nanowire arrays. Recently, carbon QD (CQD)-attached TiO_2 photoanodes were reported.[97] The CQDs electrodeposited on the TiO_2 can significantly broaden the photoresponse range of the TiO_2 to the visible and near-infrared (NIR) regions. Under the simulated AM1.5 sunlight illumination, the photocurrent density of the TiO_2/CQD photoanode was 4 times larger than the TiO_2 photoanode at 0 V (vs. Ag/AgCl).

Sensitization of metal oxide photoanodes with more than one component QDs has been investigated to further enhance PEC performance. Co-sensitization using CdS and CdSe QDs by *in situ* growth has been demonstrated for water oxidation.[98–100] The CdS and CdSe co-sensitized photoelectrodes were found to have a complementary effect in the light absorption showing a significant enhancement in photocurrents in comparison with the case using a single sensitizer (CdS or CdSe). Recently, Trevisan *et al.* demonstrated *in situ* growth of CdS and PbS QDs on mesoporous TiO_2 aiming at harvesting light in both visible and NIR regions and their application for PEC hydrogen generation.[101]

In addition to *in situ* approaches, post-synthesis assembly approaches for QD sensitization have been also investigated. In particular, the simultaneous use of QDs with different, well-controlled sizes can be realized by the post-synthesis assembly. Although *ex situ* QD sensitization methods have been widely applied to photovoltaic solar cell applications,[84,90,102] such studies for PEC water splitting are relatively scarce. Sensitization of the ZnO nanowire arrays by attaching already synthesized InP QDs with various sizes (i.e., possessing different band gaps) was demonstrated.[103] Different-size InP QDs were utilized as simultaneous sensitizers. The multi-band gap sensitization layer of InP QDs harvested complementary sunlight in the visible region, resulting in enchaced PEC efficiencies than the single-size QDs.

QD sensitization is a very effective way to extend photoanode absorption to the visible light or NIR region. However, metal chalcogenides, the most widely studied QDs, are prone to photocorrosion under water oxidation conditions due to the facile oxidation of sulfides or selenides.[11] Thus, they require sacrificial agents, which can be a serious limitation in practical solar water splitting applications. Hence, finding new QDs that are corrosion resistant but absorbing ample visible light would be a critical contribution to the field.

Surface plasmons are collective oscillations of the conduction electrons confined to the conducting material surfaces and can be excited by light. Irradiating metal nanoparticles with incident light at their plasmon frequency generates intense electric fields at the nanoparticle surface.[103] The resonance frequency can be tuned by varying the nanoparticle size, shape, material, and proximity to other nanoparticles.[104–106] The surface plasmon resonance (SPR) of metal nanoparticles has been studied to improve the PEC water splitting efficiency. Possible mechanisms for enhancing the efficiency via integration of the plasmonic metal nanoparticles with semiconductor include plasmon resonance energy transfer (PRET), photon scattering effect, hot electron transfer, plasmon-induced heating, and reflection reduction at the metal/semiconductor interface.[104,107] Among them, two mechanisms have been mainly discussed in the literature reporting plasmonic enhancement in typical PEC water splitting: PRET and hot electron injection to conduction bands of metal oxides. The PRET requires an overlap between the plasmon resonance and photon absorption of metal oxides. The electric field intensity is enhanced by PRET in the vicinity of the metal oxide, thereby increasing the power absorbed in this region. For hot electron transfer to metal oxides on the other hand, the enhancement can occur at energies well below the metal oxide band gap (i.e., sensitization).[107] The hot electrons with sufficient energies can be injected into the metal oxide conduction band.

Although α-Fe_2O_3 has been regarded as a promising candidate for water splitting photoanode materials due to its desirable band gap of 2.2 eV, photoelectrochemical stability, earth-abundance, and cost-effectiveness, α-Fe_2O_3 exhibited the inherent mismatch between the long light absorption length and the short minority carrier (hole) diffusion length. Therefore, the charge carriers generated in only a very thin layer (a few nanometers without bias and tens of nanometers with bias) near the interface with the electrolyte can contribute effectively to the water oxidation reactions on the surface of the α-Fe_2O_3 electrode.[108] The photocurrent enhancement spectra of Au/α-Fe_2O_3 were demonstrated by concentrating light near the α-Fe_2O_3/electrolyte interface to generate more photogenerated carriers (i.e., PRET and scattering effects) that can reach the interface and participate in water oxidation reactions (Figure 4(a)).[109] Gao *et al.* fabricated a thin-film α-Fe_2O_3 photoanode coated on arrays

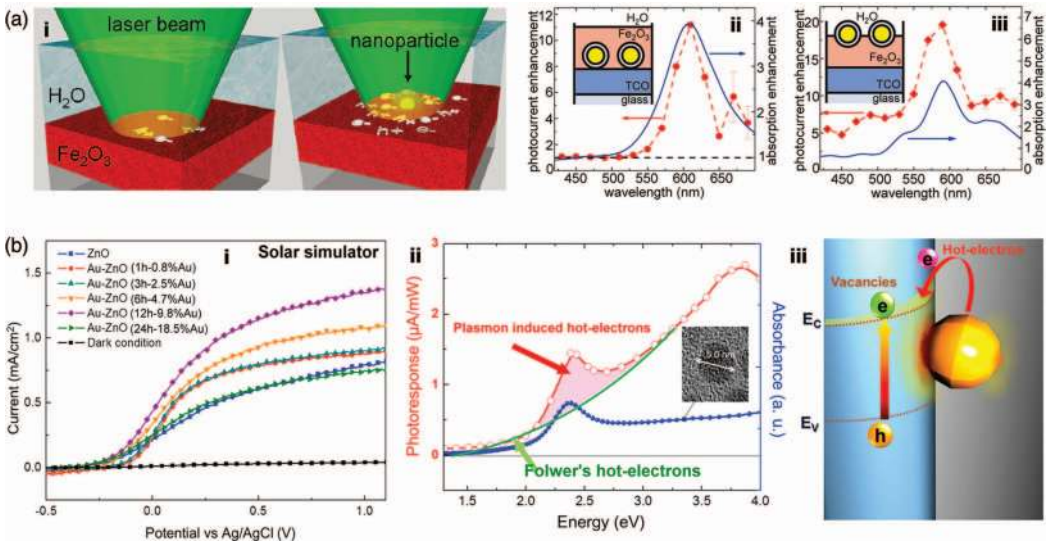

FIG. 4. (a): (i) Schematic illustration of light concentration near the semiconductor/liquid interface by metal nanoparticle. (ii and iii) Measured photocurrent (red symbols) and simulated (solid blue lines) absorption enhancement spectra that show the beneficial effects of placing silica-coated Au particles at the bottom/on top of a 100 nm α-Fe_2O_3 photoelectrode layer.[109] Reproduced by permission from I. Thomann, B. A. Pinaud, Z. B. Chen, B. M. Clemens, T. F. Jaramillo, and M. L. Brongersma, Nano Lett. **11**, 3440 609 (2011). Copyright 2011 American Chemical Society. (b): (i) Current-potential curves of ZnO/Au photoelectrodes with nanoparticles deposited for various periods. (ii) Absorption spectrum of Au nanospheres and plots of photocurrent vs. wavelength, fitted to Fowler's law, indicating that photocurrent comprises mainly hot electron flow. (iii) Schematic illustration of the plasmon-induced effects on ZnO/Au photoelectrode.[114] Reproduced by permission from H. M. Chen, C. K. Chen, C. J. Chen, L. C. Cheng, P. C. Wu, B. H. Cheng, Y. Z. Ho, M. L. Tseng, Y. Y. Hsu, T. S. Chan, J. F. Lee, R. S. Liu, and D. P. Tsai, ACS Nano **6**, 7362 (2012). Copyright 2012 American Chemical Society.

of Au nanopillars.[108] The photoanodes exhibited a net photocurrent enhancement as high as 50% over the solar spectrum at 1.5 V (vs. RHE) attributed primarily to the optical absorption increase originating from both SPR and photonic-mode light trapping in the nanostructured topography.

Ingram *et al.* reported evidence that the PRET and the scattering of photons by metal nanoparticles allows the selective formation of electron-hole pairs in the near-surface region of the semiconductor by using physical mixture of poly(vinylpyrrolidone)-encapsulated Ag nanoparticles and N-doped TiO_2.[110] The authors found that the photocurrent followed half- and first-order dependences on the intensities in the N-doped TiO_2 and Ag/N-doped TiO_2, respectively, indicating that charge carriers formed close to the N-doped TiO_2 surface in Ag/N-doped TiO_2. Liu *et al.* observed enhanced photocurrent densities in water splitting under visible light irradiation by depositing Au nanoparticles onto the visible light-active TiO_2 film (due to N and F as impurities) prepared by anodization with enhancements of up to 5-fold and 66-fold at 532 nm and 633 nm, respectively.[111] The authors attributed the enhancements to the PRET rather than the electron transfer.

Recently, significantly enhanced PEC water oxidation efficiencies under visible light irradiation have been reported by attachments of Au nanostructures to visible light-inert wide band gap metal oxides.[112–114] The reports attributed the enhancements by the Au attachments mainly to hot electron transfers to semiconductors. Zhang *et al.* demonstrated that Au nanocrystals attached to photonic crystal substrate composed of TiO_2 nanotubes yielded a photocurrent density of ca. 150 μA cm^{-2} under visible light.[112] The visible light activity was derived from the matching of the Au SPR wavelength with the band gap of the photonic crystal leading to increase in the SPR intensity that promoted hot electron injection. Pu *et al.* reported TiO_2 nanowires decorated with a mixture of Au spherical nanoparticles and nanorods that showed enhanced photoactivities in the entire UV-visible region.[113] Photovoltage experiment and 3D finite-difference time domain simulation suggested that the enhanced photoactivity was due to the PRET and surface passivation effects in the UV region and hot electron transfer from Au and partially PRET resulting from TiO_2 defect states

in the visible region. Chen *et al.* observed enhanced PEC efficiencies by coupling ZnO nanorod array photoanodes with Au nanoparticles (Figures 4(b)–4(i)).[114] The photocurrent vs. wavelength data and x-ray absorption spectroscopy result suggested the plasmon-induced hot electrons and additional vacancies created by the plasmon-induced electromagnetic field gave rise to the efficiency enhancements (Figures 4(b)-ii and 4(b)-iii).

Enhancement of the PEC efficiency in water splitting via SPR is a complex multifaceted process that requires the careful consideration of various parameters such as morphology, bandgap, band edge position, and midgap state of metal oxides and size, morphology, plasmonic particle areal density, and location of plasmonic metal nanoparticles.

Decoupling the photon absorption and water oxidation catalytic functions of the electrode to some degree can be achieved by coupling co-catalyst. Because of kinetic barriers associated with the four-electron process of water oxidation (Eq. (1)), a considerable overpotential is needed and the reaction kinetics must also compete with electron-hole recombination.[115] For practical energy conversion applications, applied potential should be reduced to lower the cost. Therefore, co-catalysts have been coupled with photoanodes in order to facilitate the water oxidation process by the following functions: (i) To make the desired reaction kinetically competitive by reducing the overpotential of the reaction; (ii) To provide a metal oxide (or metal)/electrolyte interface to enhance electron-hole separation; and (iii) To inhibit photocorrosion of photoanodes by faster charge transfer kinetics across the interface than the anodic oxidative reaction.

RuO_2 and IrO_2 are the best known catalysts for water oxidation. Despite low terrestrial abundance and the high cost of ruthenium and iridium, they are stable and highly active for water oxidation.[116–119] They have been coupled with photoanodes as co-catalysts to enhance PEC water splitting efficiencies. Deposition of RuO_2 nanoparticles onto α-Fe_2O_3 photoanodes by a spray pyrolytic method reduced the onset potential of the photocurrent by ca. 120 mV.[120] Tilley *et al.* prepared IrO_2 nanoparticle-attached α-Fe_2O_3 photoanodes.[121] The dendritic α-Fe_2O_3 nanostructure arrays were fabricated by APCVD followed by electrophoretic depostion of IrO_2 nanoparticles. The IrO_2 coupling exhibited a cathodic onset potential shift of ca. 200 mV (Figure 5(a)), achieving a STH conversion efficiency of ca. 5%. Recently, Seol *et al.* reported that modification of the cadmium chalcogenide QD-sensitized ZnO photoanode with $IrO_x \cdot nH_2O$ nanoparticles induced a cathodic shift in the onset potential, an increased photocurrent and the improved photochemical stability (Figure 5(b)).[122] Although Na_2S was used as a sacrificial agent, the system achieved a photocurrent density of 13.9 mA cm^{-2} at 0.6 V (vs. RHE) and an onset potential of −0.277 V (vs. RHE).

Cobalt-based electrocatalysts such as cobalt phosphate (Co-Pi),[123] cobalt methylphosphonate,[124] and cobalt borate[125] have emerged as affordable and efficient candidates for water oxidation catalysts.[126] They are composed of earth-abundant elements, can be easily deposited by electro- or photo-deposition methods onto a variety of electrodes from the corresponding Co^{2+} solutions in anion buffer and exhibited electrochemical O_2 evolution at relatively low overpotentials under mild ambient conditions.[11] Furthermore, the Co-Pi was found to have a "self-healing" capacity under turnover conditions in phosphate buffer.[127]

Co-Pi has been also explored for PEC water oxidation. Zhong *et al.* electrodeposited continuous thin layers of Co-Pi onto dendritic α-Fe_2O_3 films prepared by APCVD as shown in Figure 5(c).[128,129] The α-Fe_2O_3/Co-Pi photoanodes exhibited a ca. 200 mV cathodic shift in the PEC onset potential compared to that of α-Fe_2O_3 alone, like the cases of other electrocatalyst deposition such as RuO_2 and IrO_x. About 5 times enhancements in the photocurrent density and O_2 evolution rate were also observed at 1.0 V (vs. RHE) with the optimized α-Fe_2O_3/Co-Pi photoanodes.[129] Co-Pi has been also integrated with other metal oxide photoanodes, such as ZnO,[130] $BiVO_4$,[131] and WO_3,[132] showing clear cathodic shifts on onset potential. Although the phenomenological advantages of coupling Co-Pi with metal oxide photoanodes have been confirmed, the origin of the improvement is not yet fully understood.[115] Recently, two reports suggest different roles for the Co-Pi deposited on photoanodes. Barroso *et al.* suggested that Co-Pi traps electrons of α-Fe_2O_3 (instead of holes), thereby resulting in increased band bending and improved charge separation within the α-Fe_2O_3 based on the results of transient absorption measurements.[133] On the other hand, impedance and transient photocurrent spectroscopies from Klahr *et al.* suggested the oxidation of Co^{3+} to Co^{4+}

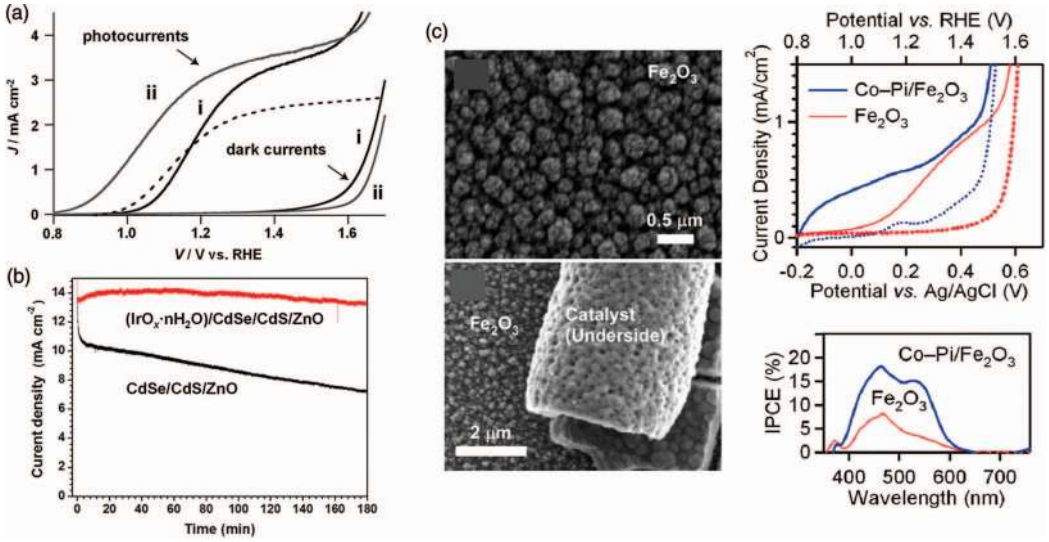

FIG. 5. (a) Current-potential curves of α-Fe_2O_3 photoanodes (i) before and (ii) after IrO_2 coupling.[121] Reproduced by permission from S. D. Tilley, M. Cornuz, K. Sivula, and M. Gratzel, Angew. Chem., Int. Ed. **49**, 6405 (2010). Copyright 2010 Wiley-VCH. (b) Chronoamperometry for CdSe/CdS/ZnO nanowire electrode before and after $IrO_x \cdot nH_2O$ modification, at 0.6 V (vs. RHE) under 1 sun simulated AM1.5 illumination.[122] Reproduced by permission from M. Seol, J. W. Jang, S. Cho, J. S. Lee, and K. Yong, Chem. Mater. **25**, 184 (2013). Copyright 2013 American Chemical Society. (c) SEM images, dark (dashed) and photocurrent (solid) densities and incident photon-tocurrent conversion efficiency spectra of mesostructured α-Fe_2O_3 photoanodes before and after electrodeposition of cobalt phosphate.[128] Reproduced by permission from D. K. Zhong, J. W. Sun, H. Inumaru, and D. R. Gamelin, J. Am. Chem. Soc. **131**, 6086 (2009). Copyright 2009 American Chemical Society.

in Co-Pi by holes photogenerated in α-Fe_2O_3 that reduced surface recombination.[134] Although the different scenarios could be speculated due to different α-Fe_2O_3 film morphologies, Co-Pi deposition methods, Co-Pi film morphologies, and characterization tools, the studies have shed light on these important questions, while also highlighting the need for further research in this area.[115]

Metal oxides, possessing high photoelectrochemical stabilities and low cost synthetic routes, are the most promising photoanode materials for practical solar water splitting. In this paper, strategies for efficient water splitting by designing metal oxides as photoanodes have been presented: (i) size and morphology-control, (ii) metal oxide heterostructuring, (iii) introducing dopants, (iv) attachments of quantum dots as sensitizer, (v) attachments of plasmonic metal nanoparticles, and (vi) co-catalyst coupling. The performance enhancements through these designed strategies are associated mainly with reduction in recombination rate, increase in conductivity, promotion of charge carrier separation, and increase in optical absorption. Some studies have reported the multiple strategy applications such as doping + QD,[135] heterostructuring + doping,[72] doping + plasmonic metal,[110] QD + co-catalyst,[122] doping + co-catalyst,[72] plasmonic metal + co-catalyst,[136] and morphology control + doping + co-catalyst.[137] Further progress is expected through further developing the presented approaches and finding novel strategies based on a more detailed understanding of materials and PEC water splitting processes. The efficient photoanodes of the future which should be ultimately integrated with photocathodes to splitting water without externally applied bias under sunlight would improve the competitiveness of this solar energy conversion technology.

This work was supported by BK+ program, and grants from Basic Science Research Program (Grant No. 2012–017247) and the Korea Center for Artificial Photosynthesis (KCAP, Grant No. 2012M1A2A2671779) funded by the National Research Foundation of Korea.

[1] J. R. Swierk and T. E. Mallouk, Chem. Soc. Rev. **42**(6), 2357 (2013).
[2] J. Z. Zhang, MRS Bull. **36**(1), 48 (2011).
[3] S. C. Tsang, J. B. Claridge, and M. L. H. Green, Catal. Today **23**(1), 3 (1995).

[4] M. T. Mayer, Y. J. Lin, G. B. Yuan, and D. W. Wang, Acc. Chem. Res. **46**(7), 1558 (2013).
[5] F. E. Osterloh and B. A. Parkinson, MRS Bull. **36**(1), 17 (2011).
[6] A. Fujishima and K. Honda, Nature (London) **238**(5358), 37 (1972).
[7] T. Bak, J. Nowotny, M. Rekas, and C. C. Sorrell, Int. J. Hydrogen Energy **27**(10), 991 (2002).
[8] K. Sivula, J. Phys. Chem. Lett. **4**(10), 1624 (2013).
[9] C. X. Kronawitter, L. Vayssieres, S. H. Shen, L. J. Guo, D. A. Wheeler, J. Z. Zhang, B. R. Antoun, and S. S. Mao, Energy Environ. Sci. **4**(10), 3889 (2011).
[10] M. G. Walter, E. L. Warren, J. R. McKone, S. W. Boettcher, Q. Mi, E. A. Santori, and N. S. Lewis, Chem. Rev. **110**(11), 6446 (2010).
[11] J. W. Sun, D. K. Zhong, and D. R. Gamelin, Energy Environ. Sci. **3**(9), 1252 (2010).
[12] J. Augustynski, B. D. Alexander, and R. Solarska, in *Photocatalysis*, edited by C. A. Bignozzi (Springer-Verlag, Berlin, 2011), Vol. 303, p. 1.
[13] Y. J. Lin, G. B. Yuan, R. Liu, S. Zhou, S. W. Sheehan, and D. W. Wang, Chem. Phys. Lett. **507**(4–6), 209 (2011).
[14] Z. S. Li, W. J. Luo, M. L. Zhang, J. Y. Feng, and Z. G. Zou, Energy Environ. Sci. **6**(2), 347 (2013).
[15] S. Choudhary, S. Upadhyay, P. Kumar, N. Singh, V. R. Satsangi, R. Shrivastav, and S. Dass, Int. J. Hydrogen Energy **37**(24), 18713 (2012).
[16] F. E. Osterloh, Chem. Soc. Rev. **42**(6), 2294 (2013).
[17] R. van de Krol, Y. Q. Liang, and J. Schoonman, J. Mater. Chem. **18**(20), 2311 (2008).
[18] A. Kudo and Y. Miseki, Chem. Soc. Rev. **38**(1), 253 (2009).
[19] J. Nelson, *The Physics of Solar Cells* (Imperial College Press, London, 2003).
[20] J. M. Spurgeon, H. A. Atwater, and N. S. Lewis, J. Phys. Chem. C **112**(15), 6186 (2008).
[21] N. Beermann, L. Vayssieres, S. E. Lindquist, and A. Hagfeldt, J. Electrochem. Soc. **147**(7), 2456 (2000).
[22] T. Lindgren, H. L. Wang, N. Beermann, L. Vayssieres, A. Hagfeldt, and S. E. Lindquist, Sol. Energy Mat. Sol. Cells **71**(2), 231 (2002).
[23] A. Wolcott, W. A. Smith, T. R. Kuykendall, Y. Zhao, and J. Z. Zhang, Small **5**(1), 104 (2009).
[24] S. U. M. Khan and T. Sultana, Sol. Energy Mat. Sol. Cells **76**(2), 211 (2003).
[25] K. S. Ahn, S. Shet, T. Deutsch, C. S. Jiang, Y. F. Yan, M. Al-Jassim, and J. Turner, J. Power Sources **176**(1), 387 (2008).
[26] A. Fitch, N. C. Strandwitz, B. S. Brunschwig, and N. S. Lewis, J. Phys. Chem. C **117**(5), 2008 (2013).
[27] S. S. Kalanur, Y. J. Hwang, S. Y. Chae, and O. S. Joo, J. Mater. Chem. A **1**(10), 3479 (2013).
[28] R. H. Goncalves, L. D. T. Leite, and E. R. Leite, ChemSusChem **5**(12), 2341 (2012).
[29] H. G. Kim, P. H. Borse, J. S. Jang, C. W. Ahn, E. D. Jeong, and J. S. Lee, Adv. Mater. **23**, 2088 (2011)
[30] O. K. Varghese and C. A. Grimes, Sol. Energy Mat. Sol. Cells **92**(4), 374 (2008).
[31] T. J. LaTempa, X. J. Feng, M. Paulose, and C. A. Grimes, J. Phys. Chem. C **113**(36), 16293 (2009).
[32] S. K. Mohapatra, S. E. John, S. Banerjee, and M. Misra, Chem. Mater. **21**(14), 3048 (2009).
[33] G. K. Mor, K. Shankar, M. Paulose, O. K. Varghese, and C. A. Grimes, Nano Lett. **5**(1), 191 (2005).
[34] M. Paulose, K. Shankar, S. Yoriya, H. E. Prakasam, O. K. Varghese, G. K. Mor, T. A. Latempa, A. Fitzgerald, and C. A. Grimes, J. Phys. Chem. B **110**(33), 16179 (2006).
[35] A. Duret and M. Gratzel, J. Phys. Chem. B **109**(36), 17184 (2005).
[36] I. Cesar, A. Kay, J. A. G. Martinez, and M. Gratzel, J. Am. Chem. Soc. **128**(14), 4582 (2006).
[37] F. Amano, M. Tian, G. Wu, B. Ohtani, and A. Chen, ACS Appl. Mater. Interfaces **3**(10), 4047 (2011).
[38] J. Yang, W. Li, J. Li, D. Sun, and Q. Chen, J. Mater. Chem. **22**(34), 17744 (2012).
[39] A. Kay, I. Cesar, and M. Gratzel, J. Am. Chem. Soc. **128**(49), 15714 (2006).
[40] L. W. Zhang, C. Baumanis, L. Robben, T. Kandiel, and D. Bahnemann, Small **7**(19), 2714 (2011).
[41] E. Yablonovitch, Phys. Rev. Lett. **58**(20), 2059 (1987).
[42] S. John, Phys. Rev. Lett. **58**(23), 2486 (1987).
[43] P. Russell, Science **299**(5605), 358 (2003).
[44] K. Ishizaki and S. Noda, Nature (London) **460**(7253), 367 (2009).
[45] J. I. L. Chen, G. von Freymann, S. Y. Choi, V. Kitaev, and G. A. Ozin, Adv. Mater. **18**(14), 1915 (2006).
[46] X. Shi, K. Zhang, K. Shin, J. H. Moon, T.-W. Lee, and J. H. Park, Phys. Chem. Chem. Phys. **15**(28), 11717 (2013).
[47] S. Nishimura, N. Abrams, B. A. Lewis, L. I. Halaoui, T. E. Mallouk, K. D. Benkstein, J. van de Lagemaat, and A. J. Frank, J. Am. Chem. Soc. **125**(20), 6306 (2003).
[48] T. Suezaki, P. G. O'Brien, J. I. L. Chen, E. Loso, N. P. Kherani, and G. A. Ozin, Adv. Mater. **21**(5), 559 (2009).
[49] S. Guldin, S. Huttner, M. Kolle, M. E. Welland, P. Muller-Buschbaum, R. H. Friend, U. Steiner, and N. Tetreault, Nano Lett. **10**(7), 2303 (2010).
[50] S. Kim, B. Fisher, H.-J. Eisler, and M. Bawendi, J. Am. Chem. Soc. **125**(38), 11466 (2003).
[51] S. Y. Kuang, L. X. Yang, S. L. Luo, and Q. Y. Cai, Appl. Surf. Sci. **255**(16), 7385 (2009).
[52] Y. Wang, T. Yu, X. Y. Chen, H. T. Zhang, S. X. Ouyang, Z. S. Li, J. H. Ye, and Z. G. Zou, J. Phys. D: Appl. Phys. **40**(13), 3925 (2007).
[53] K. J. McDonald and K. S. Choi, Chem. Mat. **23**(21), 4863 (2011).
[54] J. Yin, L. J. Bie, and Z. H. Yuan, Mater. Res. Bull. **42**(8), 1402 (2007).
[55] J. H. Park, O. O. Park, and S. Kim, Appl. Phys. Lett. **89**(16), 163106 (2006).
[56] J. Wang, Y. H. Han, M. Z. Feng, J. Z. Chen, X. J. Li, and S. Q. Zhang, J. Mater. Sci. **46**(2), 416 (2011).
[57] W. Smith, A. Wolcott, R. C. Fitzmorris, J. Z. Zhang, and Y. P. Zhao, J. Mater. Chem. **21**(29), 10792 (2011).
[58] J. Z. Su, L. J. Guo, N. Z. Bao, and C. A. Grimes, Nano Lett. **11**(5), 1928 (2011).
[59] S. J. Hong, S. Lee, J. S. Jang, and J. S. Lee, Energy Environ. Sci. **4**(5), 1781 (2011).
[60] E. S. Kim, N. Nishimura, G. Magesh, J. Y. Kim, J. W. Jang, H. Jun, J. Kubota, K. Domen, and J. S. Lee, J. Am. Chem. Soc. **135**, 5375 (2013).

[61] F. Le Formal, N. Tetreault, M. Cornuz, T. Moehl, M. Gratzel, and K. Sivula, Chem. Sci. **2**(4), 737 (2011).
[62] T. Hisatomi, F. Le Formal, M. Cornuz, J. Brillet, N. Tetreault, K. Sivula, and M. Gratzel, Energy Environ. Sci. **4**(7), 2512 (2011).
[63] Q. F. Zhang, C. S. Dandeneau, X. Y. Zhou, and G. Z. Cao, Adv. Mater. **21**(41), 4087 (2009).
[64] S. Cho, J. W. Jang, J. S. Lee, and K. H. Lee, Nanoscale **4**(6), 2066 (2012).
[65] M. Zhong, Y. B. Li, I. Yamada, and J. J. Delaunay, Nanoscale **4**(5), 1509 (2012).
[66] H. Jun, B. Im, J. Y. Kim, Y. O. Im, J. W. Jang, E. S. Kim, H. J. Kang, S. J. Hong, and J. S. Lee, Energy Environ. Sci. **5**(4), 6375 (2012).
[67] J. A. Glasscock, P. R. F. Barnes, I. C. Plumb, and N. Savvides, J. Phys. Chem. C **111**(44), 16477 (2007).
[68] Y. S. Hu, A. Kleiman-Shwarsctein, A. J. Forman, D. Hazen, J. N. Park, and E. W. McFarland, Chem. Mat. **20**(12), 3803 (2008).
[69] A. Kleiman-Shwarsctein, Y. S. Hu, A. J. Forman, G. D. Stucky, and E. W. McFarland, J. Phys. Chem. C **112**(40), 15900 (2008).
[70] K. P. S. Parmar, H. J. Kang, A. Bist, P. Dua, J. S. Jang, and J. S. Lee, ChemSusChem **5**(10), 1926 (2012).
[71] R. Asahi, T. Morikawa, T. Ohwaki, K. Aoki, and Y. Taga, Science **293**(5528), 269 (2001).
[72] H. Irie, Y. Watanabe, and K. Hashimoto, J. Phys. Chem. B **107**(23), 5483 (2003).
[73] S. Cho, J. W. Jang, K. J. Kong, E. S. Kim, K. H. Lee, and J. S. Lee, Adv. Funct. Mater. **23**(19), 2348 (2013).
[74] S. U. M. Khan, M. Al-Shahry, and W. B. Ingler, Science **297**(5590), 2243 (2002).
[75] D. O. Scanlon, C. W. Dunnill, J. Buckeridge, S. A. Shevlin, A. J. Logsdail, S. M. Woodley, C. R. A. Catlow, M. J. Powell, R. G. Palgrave, I. P. Parkin, G. W. Watson, T. W. Keal, P. Sherwood, A. Walsh, and A. A. Sokol, Nat. Mater. **12**(9), 798 (2013).
[76] J. H. Park, S. Kim, and A. J. Bard, Nano Lett. **6**(1), 24 (2006).
[77] K. S. Raja, M. Misra, V. K. Mahajan, T. Gandhi, P. Pillai, and S. K. Mohapatra, J. Power Sources **161**(2), 1450 (2006).
[78] X. L. Cui, M. Ma, W. Zhang, Y. C. Yang, and Z. J. Zhang, Electrochem. Commun. **10**(3), 367 (2008).
[79] S. Hoang, S. W. Guo, N. T. Hahn, A. J. Bard, and C. B. Mullins, Nano Lett. **12**(1), 26 (2012).
[80] X. Y. Yang, A. Wolcott, G. M. Wang, A. Sobo, R. C. Fitzmorris, F. Qian, J. Z. Zhang, and Y. Li, Nano Lett. **9**(6), 2331 (2009).
[81] Y. C. Qiu, K. Y. Yan, H. Deng, and S. H. Yang, Nano Lett. **12**(1), 407 (2012).
[82] G. Liu, L. Z. Wang, C. H. Sun, X. X. Yan, X. W. Wang, Z. G. Chen, S. C. Smith, H. M. Cheng, and G. Q. Lu, Chem. Mater. **21**(7), 1266 (2009).
[83] W. J. Jo, J.-W. Jang, K.-j. Kong, H. J. Kang, J. Y. Kim, H. Jun, K. P. S. Parmar, and J. S. Lee, Angew. Chem., Int. Ed. **51**, 3147 (2012).
[84] H. Jin, S. Choi, H. J. Lee, and S. Kim, J. Phys. Chem. Lett. **4**(15), 2461 (2013).
[85] L. J. Diguna, Q. Shen, J. Kobayashi, and T. Toyoda, Appl. Phys. Lett. **91**(2), 023116 (2007).
[86] C. H. Chang and Y. L. Lee, Appl. Phys. Lett. **91**(5), 053503 (2007).
[87] AJ Nozik, Physica E **14**(1), 115 (2002).
[88] A. Ruland, C. Schulz-Drost, V. Sgobba, and D. M. Guldi, Adv. Mater. **23**(39), 4573 (2011).
[89] P. V. Kamat, J. Phys. Chem. C **111**(7), 2834 (2007).
[90] D. F. Watson, J. Phys. Chem. Lett. **1**(15), 2299 (2010).
[91] S. G. Chen, M. Paulose, C. Ruan, G. K. Mor, O. K. Varghese, D. Kouzoudis, and C. A. Grimes, J. Photochem. Photobiol. A **177**(2–3), 177 (2006).
[92] C. W. Cheng, S. K. Karuturi, L. J. Liu, J. P. Liu, H. X. Li, L. T. Su, A. I. Y. Tok, and H. J. Fan, Small **8**(1), 37 (2012).
[93] S. Hotchandani and P. V. Kamat, J. Phys. Chem. **96**(16), 6834 (1992).
[94] Y. Tak, S. J. Hong, J. S. Lee, and K. Yong, Cryst. Growth Des. **9**(6), 2627 (2009).
[95] C. J. Lin, Y. T. Lu, C. H. Hsieh, and S. H. Chien, Appl. Phys. Lett. **94**(11), 113102 (2009).
[96] S. Cho, J. W. Jang, S. H. Lim, H. J. Kang, S. W. Rhee, J. S. Lee, and K. H. Lee, J. Mater. Chem. **21**(44), 17816 (2011).
[97] X. Zhang, F. Wang, H. Huang, H. T. Li, X. Han, Y. Liu, and Z. H. Kang, Nanoscale **5**(6), 2274 (2013).
[98] Y. L. Lee, C. F. Chi, and S. Y. Liau, Chem. Mater. **22**(3), 922 (2010).
[99] P. Rodenas, T. Song, P. Sudhagar, G. Marzari, H. Han, L. Badia-Bou, S. Gimenez, F. Fabregat-Santiago, I. Mora-Sero, J. Bisquert, U. Paik, and Y. S. Kang, Adv. Energy Mater. **3**(2), 176 (2013).
[100] G. M. Wang, X. Y. Yang, F. Qian, J. Z. Zhang, and Y. Li, Nano Lett. **10**(3), 1088 (2010).
[101] R. Trevisan, P. Rodenas, V. Gonzalez-Pedro, C. Sima, R. S. Sanchez, E. M. Barea, I. Mora-Sero, F. Fabregat-Santiago, and S. Gimenez, J. Phys. Chem. Lett. **4**(1), 141 (2013).
[102] P. V. Kamat, J. Phys. Chem. C **112**(48), 18737 (2008).
[103] H. M. Chen, C. K. Chen, C. C. Lin, R. S. Liu, H. Yang, W. S. Chang, K. H. Chen, T. S. Chan, J. F. Lee, and D. P. Tsai, J. Phys. Chem. C **115**(44), 21971 (2011).
[104] W. B. Hou and S. B. Cronin, Adv. Funct. Mater. **23**(13), 1612 (2013).
[105] S. Link and M. A. El-Sayed, J. Phys. Chem. B **103**(40), 8410 (1999).
[106] T. Atay, J. H. Song, and A. V. Nurmikko, Nano Lett. **4**(9), 1627 (2004).
[107] S. C. Warren and E. Thimsen, Energy Environ. Sci. **5**(1), 5133 (2012).
[108] H. W. Gao, C. Liu, H. E. Jeong, and P. D. Yang, ACS Nano **6**(1), 234 (2012).
[109] I. Thomann, B. A. Pinaud, Z. B. Chen, B. M. Clemens, T. F. Jaramillo, and M. L. Brongersma, Nano Lett. **11**(8), 3440 (2011).
[110] D. B. Ingram and S. Linic, J. Am. Chem. Soc. **133**(14), 5202 (2011).
[111] Z. W. Liu, W. B. Hou, P. Pavaskar, M. Aykol, and S. B. Cronin, Nano Lett. **11**(3), 1111 (2011).
[112] Z. H. Zhang, L. B. Zhang, M. N. Hedhili, H. N. Zhang, and P. Wang, Nano Lett. **13**(1), 14 (2013).
[113] Y. C. Pu, G. M. Wang, K. D. Chang, Y. C. Ling, Y. K. Lin, B. C. Fitzmorris, C. M. Liu, X. H. Lu, Y. X. Tong, J. Z. Zhang, Y. J. Hsu, and Y. Li, Nano Lett. **13**(8), 3817 (2013).

[114] H. M. Chen, C. K. Chen, C. J. Chen, L. C. Cheng, P. C. Wu, B. H. Cheng, Y. Z. Ho, M. L. Tseng, Y. Y. Hsu, T. S. Chan, J. F. Lee, R. S. Liu, and D. P. Tsai, ACS Nano **6**(8), 7362 (2012).
[115] D. R. Gamelin, Nat. Chem. **4**(12), 965 (2012).
[116] Y. X. Zhao, E. A. Hernandez-Pagan, N. M. Vargas-Barbosa, J. L. Dysart, and T. E. Mallouk, J. Phys. Chem. Lett. **2**(5), 402 (2011).
[117] Y. Lee, J. Suntivich, K. J. May, E. E. Perry, and Y. Shao-Horn, J. Phys. Chem. Lett. **3**(3), 399 (2012).
[118] N. Mamaca, E. Mayousse, S. Arrii-Clacens, T. W. Napporn, K. Servat, N. Guillet, and K. B. Kokoh, Appl. Catal. B **111**, 376 (2012).
[119] L. A. Naslund, C. M. Sanchez-Sanchez, A. S. Ingason, J. Backstrom, E. Herrero, J. Rosen, and S. Holmin, J. Phys. Chem. C **117**(12), 6126 (2013).
[120] S. A. Majumder and S. U. M. Khan, Int. J. Hydrogen Energy **19**(11), 881 (1994).
[121] S. D. Tilley, M. Cornuz, K. Sivula, and M. Gratzel, Angew. Chem., Int. Ed. **49**(36), 6405 (2010).
[122] M. Seol, J. W. Jang, S. Cho, J. S. Lee, and K. Yong, Chem. Mater. **25**(2), 184 (2013).
[123] M. W. Kanan and D. G. Nocera, Science **321**(5892), 1072 (2008).
[124] Y. Surendranath, M. Dinca, and D. G. Nocera, J. Am. Chem. Soc. **131**(7), 2615 (2009).
[125] Y. H. Lai, C. Y. Lin, Y. K. Lv, T. C. King, A. Steiner, N. M. Muresan, L. H. Gan, D. S. Wright, and E. Reisner, Chem. Commun. **49**(39), 4331 (2013).
[126] V. Artero, M. Chavarot-Kerlidou, and M. Fontecave, Angew. Chem., Int. Ed. **50**(32), 7238 (2011).
[127] D. A. Lutterman, Y. Surendranath, and D. G. Nocera, J. Am. Chem. Soc. **131**(11), 3838 (2009).
[128] D. K. Zhong, J. W. Sun, H. Inumaru, and D. R. Gamelin, J. Am. Chem. Soc. **131**(17), 6086 (2009).
[129] D. K. Zhong and D. R. Gamelin, J. Am. Chem. Soc. **132**(12), 4202 (2010).
[130] E. M. P. Steinmiller and K. S. Choi, Proc. Natl. Acad. Sci. U.S.A. **106**(49), 20633 (2009).
[131] D. K. Zhong, S. Choi, and D. R. Gamelin, J. Am. Chem. Soc. **133**(45), 18370 (2011).
[132] J. A. Seabold and K.-S. Choi, Chem. Mater. **23**(5), 1105 (2011).
[133] M. Barroso, C. A. Mesa, S. R. Pendlebury, A. J. Cowan, T. Hisatomi, K. Sivula, M. Gratzel, D. R. Klug, and J. R. Durrant, Proc. Natl. Acad. Sci. U.S.A. **109**(39), 15640 (2012).
[134] B. Klahr, S. Gimenez, F. Fabregat-Santiago, J. Bisquert, and T. W. Hamann, J. Am. Chem. Soc. **134**(40), 16693 (2012).
[135] J. Hensel, G. M. Wang, Y. Li, and J. Z. Zhang, Nano Lett. **10**(2), 478 (2010).
[136] J. Lee, S. Mubeen, X. L. Ji, G. D. Stucky, and M. Moskovits, Nano Lett. **12**(9), 5014 (2012).
[137] J. Y. Kim, G. Magesh, D. H. Youn, Y. Lee, J. Kubota, K. Domen, and J. S. Lee, Sci. Rep. **3**, 2681 (2013).